FEASIBILITY STUDY OF GAMMA-RAY MICRO-DENSITOMETRY FOR THE EXAMINATION OF NUCLEAR FUEL SWELLING

L. SENIS, V. RATHORE, P. JANSSON, P. ANDERSSON,
Department of Physics and Astronomy, Uppsala University
Regementsvägen 1, SE-752 37 Uppsala, Sweden

K. JOHNSON, D. JÄDERNÄS, C. LOSIN, D. MINGHETTI
Studsvik Nuclear AB
SE-611 82 Nyköping, Sweden

D. SCHRIRE
Vattenfall Nuclear Fuel AB
SE-169 92 Stockholm, Sweden

ABSTRACT

Nuclear fuel undergoes several thermo-mechanical changes during irradiation in a nuclear reactor, such as change of density, caused by solid and gaseous swelling. This affects the heat transport within the pellet and, when leading to the pellet-cladding gap closure, it also affects the gap conductance, causing stress in the cladding.

The density of irradiated fuel pellets can be measured in post-irradiation examination using several methods. In this work, a feasibility study was made using the gamma-ray transmission micro-densitometry technique. This is based on the comparison of two intensity measurements, with and without a sample with well-characterized thickness. Using a collimated source, a local examination of the density can be performed, scanning a pellet slice radially. The proposed technique aims to obtain a spatial resolution of cca. 100 microns.

In this work, the parameters of the setup, such as the source activity, detector counting time, slit dimensions, collimator length, and sample thickness, are used to predict detector efficiency and expected count rates. The obtainable precision of the density is assessed by first-order uncertainty propagation of counting errors in the gamma-ray detection to the density estimate.

A collimator design was presented that achieves a reasonable compromise between time requirements, precision, and spatial resolution. The sensitivity of the performance to set-up parameters was investigated. In addition, a realistic setup was modelled in MCNP6 for validation of the peak count-rate, and to ensure that the total spectrum count-rate is within typical throughput capabilities of HPGe detectors. The MCNP model was also used to confirm that the assumed attenuation law is valid in a relevant geometry, and to assess the spatial resolution, using the 10-90% edge spread of an Edge Spread Function.

It is concluded that fuel density can be determined with <1 % precision, using a 100-micron wide slit, and 1 hour of measurement.

1. Introduction

The variation of fuel properties due to irradiation is important for the safe performance of the fuel during the operation in reactors [1]. In particular, swelling phenomena [2] influence the evolution of the mechanical stress to the cladding and the heat transport [3] from the fuel to the cladding.

For UOX and MOX fuels, the swelling has been observed to be correlated with burnup [4]. The phenomenon is mainly due to the fission products that change the microscopic structure of the fuel, in particular its stoichiometry and porosity [1] [5] [6]. The fission products are generated with a well-defined yield and include both solid and gaseous species. Both cause swelling [7],

0.32-1.3% $\Delta V/V$ for the solid swelling per 1% of burnup [1], and a variable amount as a function of burnup for the gaseous case, depending on the local temperature history [6]. At the end of fuel life at typically 5% burnup, the combination of the two effects gives a total decrease of the density of about 6% on average in the whole pellet [8].
The density is not homogeneous within the pellet, both due to local variation of the fission rate and due to the subsequent evolution of the fission gasses produced. This is a complex process including migration of gasses to and from pores and release to the pellet-cladding gap [9]. In particular, high porosity has been observed in the rim region of the pellet, where the presence of high-burnup structures (HBS) [10] promotes a higher porosity fraction up to tens of percent [11]. Due to the prevailing axial symmetry of the porosity distribution, it is of interest to characterize the radial profile of the density for irradiated fuel pellets and to evaluate their heat transfer properties.
In this work, the feasibility of gamma-ray micro-densitometry for the assessment of radial density distribution in irradiated fuel samples was evaluated. Starting from the definition of the technique, the paper describes the critical parameters involved and gives a first evaluation of the instrument's performance. Due to the small changes in the density profile of irradiated nuclear fuel, a relatively good precision of the density ($\sigma_\rho/\rho < 1\%$) is needed, to resolve the density variations in the sample. It was expected that the main challenge for micro-densitometry was to allow for high enough precision in the measurement of the radiation intensity, while simultaneously having a small enough slit for a spatial resolution in the region of 100 microns, within affordable measurement time requirements.

2. Proposed setup

The instrument is planned for use in a hot cell facility in Studsvik's Nyköping (SE) laboratories and integrated within an existing hot cell structure. The setup uses an external gamma source, which irradiates a fuel sample placed on a motorized sample holder. The radiation transmitted through the sample is collimated before reaching a detector. Some assumptions made for the components of the setup are briefly described below in Sections 2.1 – 2.4. A schematic drawing of the planned setup is shown in Fig. 1.

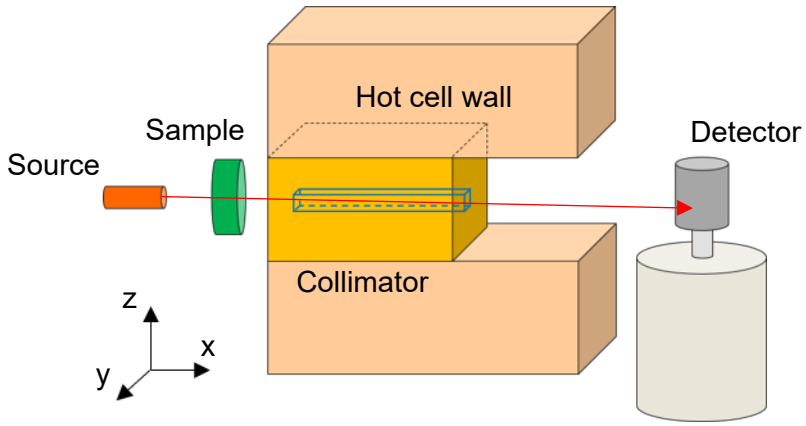

Fig 1. Not-to-scale representation of the proposed instrumental setup. The source (composed of a collection of ^{60}Co pellets) and the fuel sample are positioned within the hot cell chamber, in the proximity of the hot cell wall. The collimator is inserted into a channel penetrating the hot cell shielding. The detector is positioned outside the hot cell and is aligned with the source and with the line of sight of the collimator slit.

2.1 External source

Radioactive cylindrical pellets of ^{60}Co are available at Studsvik's facility and are planned to be used as an external source. This nuclide has two main gamma lines, at 1173 keV and 1332 keV, with nearly equal emission intensities of 99.85 % and 99.98%. The cylindrical pellets are stacked in a tube to cumulate the activities of the individual pellets. Source activity and dimensions are listed in Table 3 in Section 6.1 below.

2.2 Fuel sample

The main interest in the future use of the densitometer is for the investigation of irradiated UO_2. The as-manufactured density is expected to be near (within a few percent) the theoretical density of 10.97 g/cc. The irradiation swelling is expected to have caused variation (mainly reduction) of the density within a few percent range in most of the pellet, but up to about 20% locally in the rim [11].

The pellets will be prepared by having the upper and lower end cut off and removed. This is performed to remove the asymmetrical features of the pellet that are common in these regions, such as manufactured dishing and chamfering. The thickness of the slice after removal of the top and bottom was assumed to be at most 8 mm. As shown below in Section 3.2, the optimal thickness of a sample interrogated transmission densitometry is two attenuation lengths of the radiation (which for both gamma-ray energies of ^{60}Co is a few cm). However, for further analysis, we assumed a slice thickness at the upper limit of 8 mm. In the future, this may be reconsidered, obtaining a sample of optimal thickness by stacking multiple slices one after another.

The sample is positioned between the collimator and the source and translated by a motorized table to perform scans of the local density, by irradiating the pellet in the axial direction, at varied radial positions.

It can be noted that the correct alignment of the sample with the collimator slit is important for the performance of the setup. The length of the beam's trajectory in the sample can be evaluated using trigonometric relations and it is inversely proportional to the cosine of the misalignment angle. Supposing a reasonably small misalignment of 1°, the consequent increase of the investigated area of about 0.02%. This causes negligible effects on the planned measurements. However, the misalignment of the sample will also cause an undesired sensitivity to a broader radial range of the sample. This broadening can be also evaluated using trigonometric relations as the product of the sample thickness and the sine of the misalignment angle. Still supposing a misalignment limited to 1° and a sample thickness of 8 mm, this broadening may amount to up to 140 μm. Therefore, it can be noted that great care in the alignment is necessary to avoid degradation of the obtainable spatial resolution.

2.3 Collimator

A collimator is needed to provide sensitivity to a selected radial position of the fuel sample. High-attenuation materials, such as tungsten alloys, are ideal to stop the gamma radiation without excessive length requirements and are at the same time practical to machine. For our evaluation of the feasibility, we have assumed pure tungsten for simplicity, of density 19 g/cc.

While the shape of the collimator design may later be subject to practical reconsiderations during the manufacturing process, we have assumed a quadratic slit cross-section through a solid block of tungsten. The slit dimensions govern the spatial resolution and make it possible to perform densitometry to a microscopic scale. For our studied case, a 100-micron by 100-micron quadratic slit has been assumed. The length of the collimator was selected with the consideration that strong attenuation is required for unwanted gamma rays from outside the slit. For this purpose, the capability of attenuation for a 150 mm length collimator was evaluated using Monte Carlo radiation transport, as described in Section 6.

2.4 Detector

The collimated gamma-ray intensity will be measured using a High Purity Germanium (HPGe) coaxial detector (model Ortec GEM 25P4-70-PL already present in-situ**)**. An HPGe detector is well capable to resolve the dual peak spectrum of ^{60}Co, thanks to its high-energy resolution (1-2 keV) [12], and this is an advantage for the analysis since it allows for use of both the gamma ray lines of the ^{60}Co source.

It can be noted that for this feasibility study, we only evaluated the lower energy line of 1173 keV. The higher 1332 keV peak can be also used to provide additional data, having equal value for density analysis, but for simplicity it was not considered in this work. The assumed dimensions of the detector are reported in Table 1.

HPGe Diameter	70 mm
HPGe Height	134 mm
Dead layer thickness	0.7 mm
Aluminium Endcap distance	5 mm
Aluminium Endcap thickness	1.5 mm
Core cavity Diameter	8 mm
Core cavity depth	30 mm
Peak efficiency at 1173 keV	26.85 %

Tab 1: HPGe coaxial detector parameters of consequence for the feasibility study.

The intrinsic peak efficiency stated in Table 1 was estimated using the pulse height distribution tally in MCNP6 [13] for 1173 keV gamma rays. The geometry for the MCNP6 simulation is shown in Figure 3, Section 5.

3. Principles of operation

3.1 Transmission densitometry

The use of attenuated flux of gamma-rays for density measurements is a proven concept [14] and it is extensively used in different applications [15] [16], especially in the oil industry [17]. The technique relies on the evaluation of the attenuation of a well-defined gamma-flux caused by a sample in the path of the rays.

The function which describes the phenomenon is the Beer-Lambert law [18], shown in Eq. (1), applied to high-energy photons. This law correlates the gamma intensity generated by a collimated mono-energetic gamma source, I_0, to the intensity transmitted when a sample is present, I, as

$$I = I_0 e^{-\mu(E_\gamma)x}. \quad (1)$$

Since the gamma-ray intensity is proportional to the detector live count rate, for further considerations, we will consider I to mean the count rate of the detected gamma-rays in the full energy peak of the detector. The variation of the count rate depends on the linear attenuation coefficient, μ, and the sample thickness, x. The coefficient μ is dependent on the sample material and the gamma-ray energy, E_γ. This can be evaluated using the measured count rates as,

$$\mu(E_\gamma) = \frac{\ln {}^{I_0}/_{I}}{x}. \quad (2)$$

We can note that the linear attenuation coefficient is for practical reasons often expanded as the product of the mass attenuation coefficient, $\mu_m(Z, E_\gamma)$, - which can be extracted from libraries, such as XCOM [19] - and the sample density, ρ,

$$\mu(E_\gamma) = \rho * \mu_m(E_\gamma). \quad (3)$$

From combining Eqs. (2) and (3), is possible to calculate the sample density in this simplified case as,

$$\rho = \frac{\ln {}^{I_0}/_{I}}{x\, \mu_m(E_\gamma)}, \quad (4)$$

after measuring the un-attenuated and the attenuated count rates, and knowing the sample thickness.

4. Feasibility evaluation method

Since the measurement of the radiation intensity is an inherently discrete operation, where a certain number of counts, N, are collected during the experiment, it is subject to the well-known

counting noise that follows the Poisson distribution [20] [12], with standard deviation, $\sigma_N = \sqrt{N}$. Since the count rate is determined based on the number of counts per unit time, $I = N/t$, the relative uncertainty of the intensity decreases with the total number of counts in the peak of interest. For the feasibility study, this counting uncertainty can be considered as the ultimate limiting minimal source of uncertainty, since it is impossible to avoid or correct by calibration.
The relative uncertainty of the density was calculated using first-order error propagation theory considering the two quantities not correlated, on Eq. (4),

$$\frac{\sigma_\rho}{\rho} = \frac{\sqrt{\frac{1}{I_0 t_0} + \frac{1}{It}}}{\ln\left({}^{I_0 t_0}/_{It}\right)}. \tag{5}$$

Considering the non-attenuated gamma-flux, I_0, as a function of the planar source activity concentration, A_S, the gamma line emission probability, I_γ , the detector efficiency (intrinsic peak efficiency) at the used energy, ε_d, and the collimator transmission efficiency, ε_{coll}, the un-attenuated count rate can be estimated according to Eq. (6).

$$I_0 = A_S \, I_\gamma \, \varepsilon_{coll} \, \varepsilon_d. \tag{6}$$

The efficiency of transmission through the collimator was estimated according to the optical model for rectangular slits from ref [21],

$$\varepsilon_{coll} = \frac{w^2 h^2}{4\pi L^2}, \tag{7}$$

where w and h are respectively the width and the height of the slit, and L is its length. This collimator model is an idealization, where the bulk material is assumed to be a perfect absorber. It can be noted that this leads to an underestimation of the count rate since gamma rays can be transmitted through the collimator bulk material to some degree [21].
The planar activity concentration in front of the collimator, A_S, of Eq. (6), requires calculation based on the total activity A, and the cross-sectional area of the source (as seen from the detector orientation),

$$A_S = \frac{CA}{\pi r_{Source}^2}, \tag{8}$$

This is considering the source as a circle with a radius equal to the source pellet radius, r_{Source}. In addition, a correction factor, C, is applied in Eq. (8) to account for self-attenuation in the source. It can be shown that for an extended source with homogeneous activity and attenuation, the self-attenuation correction factor is,

$$C = \frac{1}{\mu_{Source} x_{Source}} \left(1 - \mathrm{e}^{-\mu_{Source} x_{Source}}\right), \tag{9}$$

where μ_{Source} is the linear attenuation coefficient of the cobalt source, and x_{Source} is the axial source length.

4.1 Effect of parameter variation

It can be noted that the arithmetic expressions involved in the estimation of the relative uncertainty of the density (Eq. (5) and (6)), show how density scales with the experimental parameters. The dependencies are shown in Table 2 below.

Parameter	Effect on density precision
Source Activity	$\frac{\sigma_\rho}{\rho} \sim \frac{1}{\sqrt{A}}$

Measurement time	$\frac{\sigma_\rho}{\rho} \sim \frac{1}{\sqrt{t}}$
Collimator length	$\frac{\sigma_\rho}{\rho} \sim L$
Slit dimensions	$\frac{\sigma_\rho}{\rho} \sim \frac{1}{wh}$

Tab 2: Summary of the effect of the different parameters on the density relative uncertainty.

A special case of interest is the effect of fuel sample thickness on the relative uncertainty of the density. Since it can be cut where desired, the slice thickness can be optimized. For very small thickness, the attenuation effect may be small compared to the counting noise, causing large imprecision in the measurement. In the opposite limit, with large sample thickness, the transmitted signal is almost completely attenuated, leading also to large imprecision. Consequently, there is a local optimum of the fuel sample thickness between the extremes. The minimum can be calculated differentiating Eq. (5) and is located at $x_{optim} = \frac{2}{\mu}$. For our application (for 1173 keV gamma rays in UO_2) the optimal length is about 30 mm. However, as mentioned in Section 2, a single pellet with removed top and bottom was assumed to be limited to the thickness of at most 8 mm.

4.2 Considerations of accuracy

The density precision model of Section 4 considers only the unavoidable statistical uncertainty derived from counting statistics. However, in a realistic measurement scenario, several effects may also affect the accuracy of the density measurements, generating bias in the result. Some potential sources of error that have been identified are listed below:

I. Background radioactivity: because the densitometer will be placed in a nuclear facility, there is a high likelihood that the measurements are subjected to unwanted background radiation.
II. Mass-attenuation alteration: due to irradiation, part of the fuel is converted to fission products, that alter the mass attenuation coefficient of the sample to a lower effective mass number [22]. The effect increases with the increase of local burnup. From ref [22] it is known that this can change by about 1% in nuclear fuel for 1173 keV gamma rays.
III. Coherent scattering: Coherent scattering is a minority interaction for the gamma-ray energy under consideration (about 3.6 % of the total photon cross-section). However, due to unchanged energy and only slightly altered direction, coherent scattered gammas may still reach the detector and be counted, thereby causing an alteration of the effective attenuation coefficient.
IV. Transmission through collimator material: due to the highly penetrating property of gamma rays, some source intensity can be expected to enter the detector from paths that go outside of the intended collimator slit. This fraction of the total intensity will thus not depend on the local density in the fuel sample.
V. Sample thickness uncertainty: the sample preparation and the thickness precision are important for a successful densitometry measurement. The relative uncertainty of the thickness is a factor that directly affects the density precision, being mathematically summed to Eq. (5). If in the preparation of the sample slice, the relative precision of the thickness is bigger than 1% (equal to 80 μm for the assumed slice thickness of 8 mm), this may dominate the relative uncertainty of the density. Therefore, careful sample preparation will be a priority.

It can be noted that the results of the precision evaluation using the theoretical approach according to Section 4, and with results shown in Section 6.1 do not consider any effects I-V listed above. However, it is believed that the magnitude of these inaccuracies is small and they can be corrected with a calibration routine, using samples of known density. In addition, the effects on the accuracy of bullets III and IV were evaluated by Monte Carlo modeling of a preliminary setup geometry, described below in Section 5.

5. MCNP simulations

A realistic MCNP model [13] was made for evaluation of the pulse build-up component and the full-energy gamma peak expected, in two configurations: with and without the slit. The results were used to benchmark the count-rate estimates of the theoretical feasibility evaluation and to evaluate the magnitude of the unwanted full-energy gammas reaching the detector from transmission through the collimator bulk. The total count rate obtained was also compared with the saturation limitations of the HPGe detectors (usually expected for rates higher than 10^5 events per second). A schematic drawing of the MCNP model is shown in Figure 3. The model was also used to verify the performance of the setup, including a more complete simulation of the physics of the problem (e.g scattering).

The evaluations regard the validity of the Beer-Lambert law and the spatial resolution of the setup, obtained from the Edge Spread Function (ESF). The Beer-Lambert law validity was validated using a target of pure UO_2 (50x50x10 mm rectangular plate) positioned in front of the slit and irradiated with a mono-energetic gamma-source (@ 1173 keV). The simulations were performed varying the target density from 4.5 to 11.25 g/cc with 13 density steps, and the gamma ray intensity with and without the sample was used to calculate the simulated density according to Eq. (4). The results were compared with the known model inputs.

The spatial resolution of the system was investigated using the ESF of a tungsten target (50x50x10 mm rectangular plate) with a sharp edge. The edge of the target was positioned 0.1 mm off the center of the slit and moved with a 0.005 mm step, measuring the variation of the detector count rate in 40 positions. This is expected to decrease reaching the minimum when the slit gets completely covered, causing a smear of the edge in the recorded profile. The 10-90% edge spread is used to quantify the spatial resolution.

To speed up the simulations variance reduction techniques were used. For the count rate validation, the source emission was biased in a cone centered on the slit direction, similarly to [21]. The cone central angle was set wide enough to illuminate the whole slit even from the radial periphery of the source. For validation of the Beer-Lambert idealization, and the evaluation of the ESF, an energy cut was set, slightly below the gamma emission energy, killing the gammas below 1150 keV of energy.

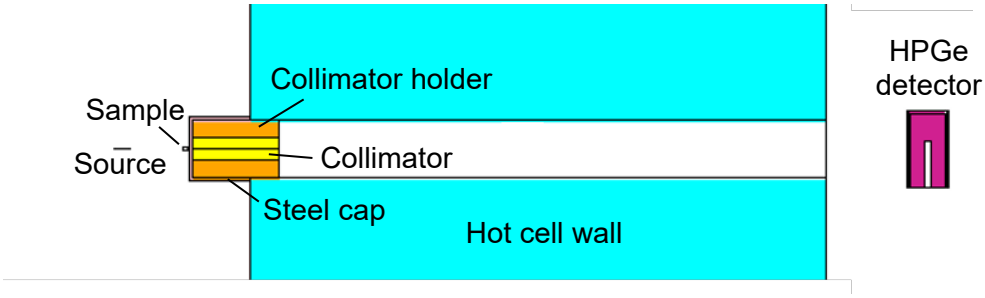

Fig 3. MCNP realistic representation of the model. Inside the hot cell are placed the source and the sample, while a steel cap separates the in and out-cell environments. The collimator and its lead holder are sited in the cap, inside the measurement channel, and at its end, the HPGe detector is positioned, and its center is aligned with the collimator slit.

6. Results

6.1 Estimated performance

Using Eq. (5) in Section 4, the predicted performance in the density precision was estimated for the planned densitometer. For this purpose, all relevant parameters needed are listed in Table 3 below. In addition, a measurement time requirement of 1 h per position is assumed.

Cobalt activity, A	1.08 TBq
Length of cobalt source, x_{Source}	27.2 mm
Source radius, r_{Source}	0.4 mm
1173 keV emission intensity, I_γ	0.9985

Fuel sample thickness, x	8 mm
Collimator slit width, w	100 µm
Collimator slit height, h	100 µm
Collimator length, L	150 mm
Measurement time, t	1 h
Measurement time, t_0	1 h
Count rate without sample, I_0	117.7 counts/s
Count rate with the sample, I	67.4 counts/s

Tab 3: Summary of all geometrical parameters of importance in the feasibility study, and assumed values in evaluation performance of proposed densitometer system.

The resulting relative uncertainty of the density was $\frac{\sigma_\rho}{\rho} = 0.46\%$. This is considered as an acceptable precision to resolve variations of the radial density. Therefore, the dimensions and experimental parameters according to Table 1 above are proposed.

6.2. MCNP results

6.2.1 Count rate prediction of a mono-energetic gamma line

Two spectra were collected in the configuration with and without the slit and the count rate was calculated for the total spectrum and the full energy peak at 1173 keV. The results are shown in Table 4. It can be noted that in the simulated case without a slit, the intensity of full-energy gamma rays in the detector is about 3% of the simulation with the planned slit. The small fraction of gamma rays originating from outside the slit is expected to have a limited effect on the measurements. Thereby, the suitability of a 150 mm long collimator of tungsten was confirmed.

The total count rate based on MCNP results is 570.5 counts/s in the slitted configuration, which is two orders of magnitude below the usual HPGe throughput limitations (10^5 events per second). Even considering the addition of another ^{60}Co gamma line at 1332 keV of nearly equal intensity, no throughput-related problems are expected with the proposed geometry.

	With slit	Without slit
Full-energy peak [counts/s]	123.8 ± 3.9	4.0 ± 0.7
Total count [counts/s]	570.5± 8.4	126.7± 3.6

Tab 4: Peak and total count rates from the MCNP simulation, of the un-attenuated beam. Results from the collimator with as proposed slit are compared with a solid collimator without a slit, confirming that the length of the collimator using is sufficient to effectively stop unwanted radiation paths.

The peak count rate based on MCNP was 5% higher than theoretically predicted according to Section 4. This minor deviation was expected, due to the possibility of full-energy gammas reaching the detector through the collimator bulk material without interacting. These were neglected in the collimator transmission model of Eq. (7), but are present in the MCNP simulation.

6.2.2 Validation of performance

The MCNP model was used to test the Beer-Lambert law validity for different input densities. The results plotted in Figure 4 show a discrepancy lower than 1.5% between the calculated and the input densities in the density range of interest, i.e. between 9 to 11 g/cc. This can likely be attributed to the transmission through the collimator and may be accounted for in the planned setup by calibration of the instrument, using samples of known density and thickness. The ESF, obtained by MCNP simulation of a scan of an object with a sharp edge is shown in Figure 4, evaluated as described in Section 5. The 10-90% edge spread was found at 110 µm, which is in good agreement with the chosen slit width, confirming a spatial resolution of about 100 µm. The same method has also been applied for a target with a rotation of 1°, accounting

for the possible event of misalignment between sample and collimator. In this case, the ESF 10-90% degrades, increasing to about 170 µm (55% more than the perfectly aligned case).

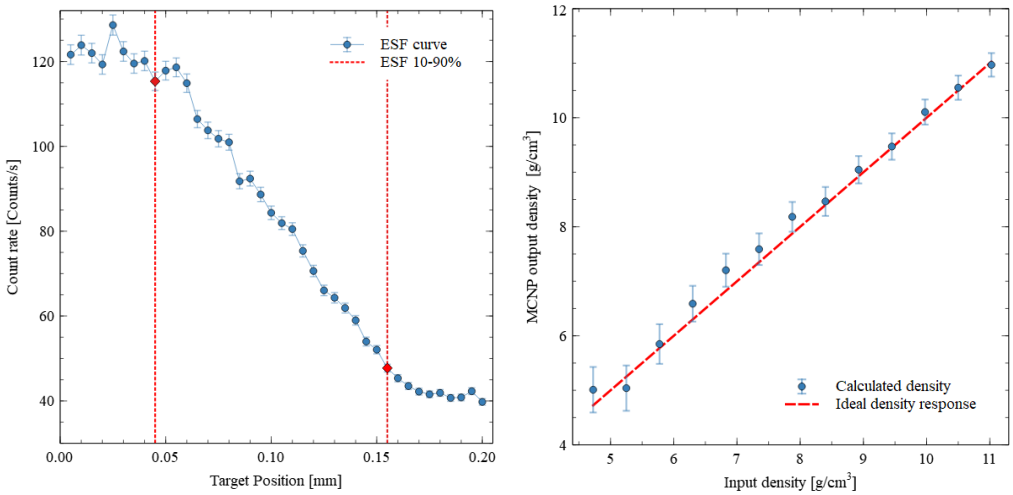

Fig 4. On the left: the ESF is plotted for different positions of the target. The 10-90% edge spread of the signal is marked in red. The distance between the two is defined by the spatial resolution of the setup. On the right: the plot shows the comparison between the calculated densities using Eq. (4) and the simulation input densities.

7 Conclusions and Outlook

A feasibility study was made of gamma-ray micro-densitometry for measuring radial swelling profiles in irradiated nuclear fuel pellets. Using theoretical models for prediction of count rate, including an optical field of view model for the collimator, and using propagation of counting uncertainties to uncertainties of the density, it was found that a density precision of 0.5%, with a spatial resolution of 100 µm, and interrogation time requirements of 1 h per position, is feasible.

The performance of the setup was validated by MCNP simulations, which showed an increase of 5% in the full-energy peak counts, which may be attributed to the transmission through the collimator material. This confirmed that the theoretical model was good enough for performing the design of the setup. The total spectrum count rate in the detector was found to be in the order of 1000 counts per second. Although this was for simplicity performed with only the 1173 keV gamma-ray from ^{60}Co and neglecting the 1332 keV gamma rays with nearly equal intensity, it can be concluded that the count rate is far lower than the throughput limitations of standard HPGe detectors.

Some sources of inaccuracy were neglected, meaning that calibration will be needed in the final setup, by measurements of samples with known density and thickness. The spatial resolution was confirmed with an MCNP simulation of the Edge Spread Function, resulting in a 10-90% edge spread of 110 µm for a collimator slit width of 100 µm.

While the local radial density may be measured with high spatial resolution using the densitometry technique as proposed in this work, it can be noted that any variations in the sample of the axial density will inevitably be averaged. No axial resolution can be obtained within the axial length of the sample (currently proposed to about 8 mm). While due to the prevailing axial symmetry in nuclear fuel rods, this is not perceived to be a large concern, it might be noted as a limitation of the proposed technique. The axial uniformity of the object under study might therefore need to be considered in the future use of the technique.

Based on the feasibility study, the construction of a hot cell wall densitometer has been started at Studsvik Nuclear AB, and it is expected that the micro-densitometer will be in operation within 2021, providing data on the radial density profile of irradiated fuel pellets.

8 Acknowledgment

This work was financially supported by the Swedish Foundation for Strategic Research, grant number EM-16-0031.

Bibliography

[1] M.F. Lyons, R.F. Boyle , J.H. Davies, V.E. Hazel and T.C. Rowland , "UO2 Properties affecting Performance," *Nuclear Engineering and design,* vol. 21, pp. 167-199, 1972, https://doi.org/10.1016/0029-5493(72)90072-6.

[2] D. Schrire, A. Kindlund and P. Ekberg, "OECD Halden Reactor Project, Enlarged Halden Programme Group Meeting on High Burn-up Fuel Performance, Safety and Reability and Degradation of In-Core MAterials and Water Chemistry Effects, vol I," HPR-349, Lillehammer, Norway, 15-20 March 1998, URL http://inis.iaea.org/Search/search.aspx?orig_q=RN:35048536.

[3] M. Amaya, M. Hirai, H. Sakurai, K. Ito, M. Sasaki, T. Nomata, K. Kamimura and R. Iwasaki, "Thermal Conductivities of Irradiated UO2, and (U,Gd)O2 Pellets," *Journal of Nuclear Materials,* vol. 300, no. 1, pp. 57-64, 2002, https://doi.org/10.1016/S0022-3115(01)00704-8.

[4] R. C. Daniel, M. L. Bleiberg, H. B. Meieran and W. Yeniscavich, "Effects of High Burnup on Zircaloy-Clad Bulk UO2, Plate Fuel Element Samples," United States, 1962, URL https://www.osti.gov/biblio/4747035.

[5] R.H. Cornell, "An Electron Microscope Examination of Matrix Fissio-Gas Bubbles in Irradiated Uranium Dioxide," *Journal of Nuclear Materials,* vol. 38, no. 3, pp. 319-328, 1971, https://doi.org/10.1016/0022-3115(71)90061-4.

[6] P. Garcia, G. Carlot, B. Dorado, S. Maillard, G. Martin, J.Y. Oh, C. Sabathier and M.J. Welland, "Mechanisms of microstructural changes of fuel under irradiation," in *in State-of-the-Art Report on Multi-scale Modelling of Nuclear Fuels*, NEA, 2015, URL http://inis.iaea.org/Search/search.aspx?orig_q=RN:47032407, pp. 22-58.

[7] L. Van Brutzel, R. Dingreville and T.J. Bartel, "Nuclear fuel deformation phenomena," in *in State of the Art Report on Multi-scale Modelling of Nuclear Fuels*, 2015, URL https://inis.iaea.org/search/search.aspx?orig_q=RN:47032408, pp. 59-79.

[8] M. Marchetti, D. Laux, L. Fongaro, T. Wiss, P. Van Uffelen, G. Despaux and V.V. Rondinella, "Physical and mechanical characterization of irradiated uranium dioxide with a broad burnup range and different dopants using acoustic microscopy," *Journal of Nuclear Materials,* vol. 494, pp. 322-329, 2017, https://doi.org/10.1016/j.jnucmat.2017.07.041.

[9] M. Szuta, "Transient Fission Gas Release from UO2 Fuel for High Temperature and High Burnup," in *Technical committee meeting on nuclear fuel behaviour modelling at high burnup and its experimental support* , Windermere (United Kingdom), 2000, URL https://www.osti.gov/etdeweb/biblio/20191518.

[10] V.V. Rondinella and T. Wiss, "The high burn-up structure in nuclear fuel," *Materials today,* vol. 13, no. 12, pp. 24-32, 2010, https://doi.org/10.1016/S1369-7021(10)70221-2.

[11] J. Spino, J. Rest, W. Goll and C.T. Walker, "Matrix swelling rate and cavity volume balance of UO2 fuels at high burn-up," *Journal of Nuclear Materials,* vol. 346, no. 2, p. 131–144, 2005, https://doi.org/10.1016/j.jnucmat.2005.06.015.

[12] G.R. Gilmore, Practical Gamma-ray Spectroscopy, Nuclear Training Services Ltd, Warrington, UK: Wiley, 2008.

[13] C.J. Werner , "MCNP Users Manual - Code Version 6.2", report LA-UR-17-29981, Los Alamos National Laboratory, 2017.

[14] G. D. Lassahn, A. G. Stephens,D. J. Taylor and D. B. Wood, "X-Ray and Gamma Ray Transmission Densitometry," in *International colloquium on densitometry*, Idaho Falls, ID, USA, 1979, URL http://inis.iaea.org/Search/search.aspx?orig_q=RN:11500068.

[15] R. R. W. Affonso, A. X. da Silva and C. M. Salgado, "Gamma ray densitometry techniques for measuring of volume fractions," in *INAC 2015: international nuclear atlantic conference. Brazilian nuclear program. State policy for a sustainable world*, Sao Paulo, SP (Brazil), 2015, URL https://inis.iaea.org/search/search.aspx?orig_q=RN:47035607.

[16] S.A. TjugumJoop, J. Frieling and G.A. Johansen, "A compact low energy multibeam gamma-ray densitometerfor pipe-flow measurements," *Nuclear Instruments and Methods in Physics Research B,* vol. 197, no. 3, p. 301–309, 2002. https://doi.org/10.1016/S0168-583X(02)01481-7.

[17] W.A.S. Kumara, B.M. Halvorsen and M.C. Melaaen, "Single-beam gamma densitometry measurements of oil–water flow," *International Journal of Multiphase Flow,* vol. 36, no. 6, p. 467–480, 2010, https://doi.org/10.1016/j.ijmultiphaseflow.2010.02.003.

[18] D.F. Swineharf, "The Beer-Lambert Law," *J. Chem. Educ.,* vol. 39, no. 7, pp. 333-335, 1962, https://doi.org/10.1021/ed039p333.

[19] M. J. Berger, J.H. Hubbell, S.M. Seltzer, J. Chang, J.S. Coursey, R. Sukumar,D.S. Zucker and K. Olsen, "XCOM: Photon Cross Section Database (version 1.5)," Gaithersburg, 2020.

[20] G.F. Knoll, Radiation Detection and Measurement, New York: Wiley, 1979.

[21] L. Senis, V. Rathore, A. Anastasiadis E. Andersson Sundén, Z. Elter, S. Holcombe, A. Håkansson, P. Jansson, D. LaBrier, J. Schulthess, P. Andersson, "Evaluation of gamma-ray transmission through rectangular collimator slits for application in nuclear fuel spectrometry," submitted for publication.

[22] H. Atak, A. Anastasiadis, P. Jansson, Z. Elter, E. Andersson Sundén et al., "The degradation of gamma-ray mass attenuation of UOX and MOX fuel with nuclear burnup," *Progress in Nuclear Energy,* vol. 125, p. 103359, 2020, https://doi.org/10.1016/j.pnucene.2020.103359.